

Ultrafast Two-Dimensional Infrared Spectroscopy of a Quasifree Rotor: J Scrambling and Perfectly Anticorrelated Cross Peaks

Aritra Mandal,^{1,3,†} Greg Ng Pack,^{1,3} Parth P. Shah,^{1,3} Shyamsunder Erramilli,^{2,3} and L. D. Ziegler^{1,3,*}

¹Department of Chemistry, Boston University, Boston, Massachusetts 02215, USA

²Department of Physics, Boston University, Boston, Massachusetts 02215, USA

³Photonics Center, Boston University, Boston, Massachusetts 02215, USA



(Received 5 August 2017; published 9 March 2018)

Ultrafast two-dimensional infrared (2DIR) spectra of the N_2O ν_3 mode in moderately dense SF_6 gas exhibit complex line shapes with diagonal and antidiagonal features in contrast to condensed phase vibrational 2DIR spectroscopy. Observed spectra for this quasifree rotor system are well captured by a model that includes all 36 possible rovibrational pathways and treats P ($\Delta J = -1$) and R ($\Delta J = +1$) branch resonances as distinct Kubo line shape features. Transition frequency correlation decay is due to J scrambling within one to two gas collisions at each density. Studies of supercritical solvation and relaxation at high pressure and temperature are enabled by this methodology.

DOI: 10.1103/PhysRevLett.120.103401

Over the last two decades, ultrafast two-dimensional infrared (2DIR) spectroscopy has emerged as one of the leading techniques for investigation of molecular structure and dynamics in condensed phases [1,2]. 2DIR spectral analysis yields information on molecular fluctuation time scales and mechanisms responsible for IR absorption line shapes, the coupling of resonant intra- or intermolecular modes or the dynamics of chemical exchange between interconverting molecular configurations or species [1–17]. For a single vibrational resonance the 2DIR spectrum consists of two oppositely signed features: ground state bleach and stimulated emission (GSB-SE) contributions centered along the diagonal, and an excited vibrational state absorption (ESA) contribution shifted along the probe frequency axis by the vibrational anharmonicity. Molecular fluctuation time scales due to bath interactions in these condensed phase systems are revealed by the waiting time (T_w) dependence of the 2DIR line shapes and correspond to the transition frequency-frequency correlation function (FFCF) of a resonantly excited vibrational mode [18].

We report here the first observations and analysis of 2DIR spectra of a quasifree quantum rotor in a moderately dense gaseous medium. 2DIR spectra of the resonantly excited ν_3 asymmetric stretching rovibrational band of N_2O in SF_6 at two densities ($\rho^* = \rho/\rho_c = 0.16$ and 0.30 ; $\rho_c = 0.74$ g/mL = 5.79 M) have been obtained. Aside from providing a rovibrationally specific framework for understanding the observed complex 2DIR spectral line shapes, these spectra demonstrate a new capability for measuring ultrafast rovibrational relaxation dynamics in the absence of discrete rotational resolution. Furthermore, characterization of the quasifree rotor 2DIR spectrum is required for studies of solvation in higher density solutions where critical point fluctuation dynamics may be evident ($\rho^* \sim 1$) and for learning about the onset of liquidlike character ($\rho^* > 1$) as a function of density.

The FTIR (Fourier transform infrared) spectrum of the N_2O ν_3 mode at $T = 313$ K in 26 atm of SF_6 ($\rho^* = 0.30$, 2.6% N_2O) is shown in Fig. 1. The corresponding spectrum of N_2O in lower density SF_6 (17 atm, $\rho^* = 0.16$, 4% N_2O) is slightly narrower. (See Supplemental Material [19], Fig. S1). The maxima at 2211 and 2236 cm^{-1} correspond to the unresolved P ($\Delta J = -1$) and R ($\Delta J = +1$) rovibrational branches, respectively, originating from the thermalized ensemble of initial rotational levels, J . The pure ($\Delta J = 0$) $0 \rightarrow 1$ ν_3 vibrational transition, i.e., the Q branch, would be centered at ~ 2224 cm^{-1} but is formally forbidden for a linear molecule in free space [20,21]. The rovibrational structure for this single vibrational resonance (Fig. 1) stands in contrast to the single maximum line shape

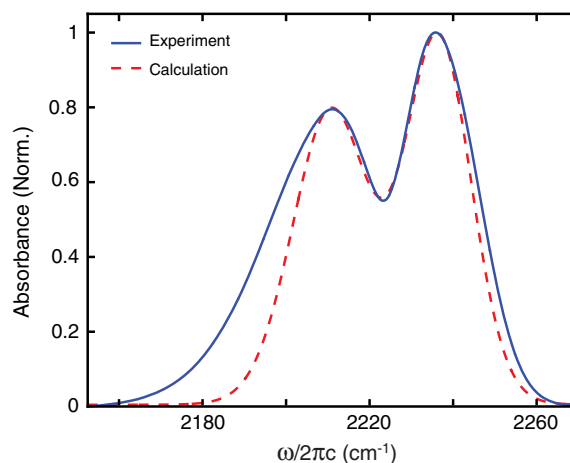


FIG. 1. Observed (solid) and modeled (dashed) FTIR spectra of the ν_3 asymmetric stretching fundamental of N_2O in $\rho^* = 0.30$ SF_6 . P and R branch maxima are at 2211 and 2236 cm^{-1} .

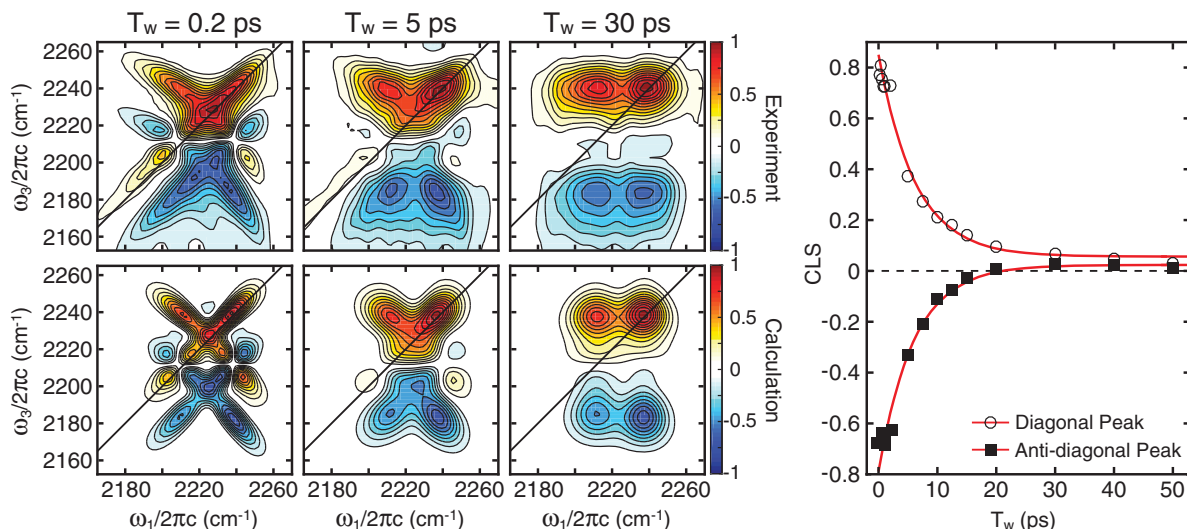


FIG. 2. Experimental and calculated 2DIR spectra of the $\text{N}_2\text{O } \nu_3$ fundamental in $\rho^* = 0.30$ SF_6 for waiting times (T_w) of 0.2, 5, and 30 ps. Frequency-frequency correlation functions determined by CLS decay for the bleach diagonal (open circle) and antidiagonal (filled square) 2DIR features and best fits to an exponential decay and a small constant offset are shown (red). The dominant decay times are 6.1 ± 0.3 ps (diagonal) and 5.8 ± 0.4 ps (antidiagonal).

observed for the $\text{N}_2\text{O } \nu_3$ transition in liquid solutions (See Fig. S1) [22].

The corresponding observed 2DIR spectra of the $\text{N}_2\text{O } \nu_3$ mode in SF_6 ($\rho^* = 0.30$) are shown in Fig. 2 for $T_w = 0.2$, 5.0, and 30 ps. These spectra were acquired in a pump-probe configuration [23], and thus rephasing and nonrephasing signals are overlapped at the detector. Perpendicularly polarized 85 fs pulses (FWHM 250 cm^{-1}) centered at $\sim 2230 \text{ cm}^{-1}$ were used to acquire these spectra. The rapid scan, phase corrected coherence delay between the first two pump pulses (τ_1) was Fourier transformed to give the ω_1 axis and the dispersed signal on a 32 element array ($\sim 3 \text{ cm}^{-1}/\text{pixel}$) corresponds to the ω_3 axis [23]. (See Supplemental Material [19] for additional experimental details). The T_w dependent 2DIR spectra of the lower density ($\rho^* = 0.16$) $\text{N}_2\text{O}/\text{SF}_6$ mixture have a qualitatively similar appearance (Fig. S2 [19]). The $\nu_3 v = 1$ lifetimes in these solutions, determined by magic angle pump-probe responses, ($\rho^* = 0.30$; 35 ps and ~ 1 ns, and for $\rho^* = 0.16$; 101 ps and ≥ 10 ns) are much slower than the dynamics revealed in these 2DIR spectra.

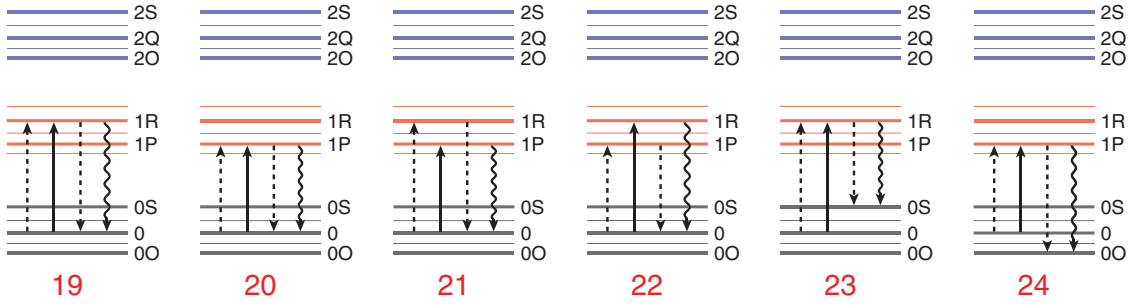
The quasifree rotor 2DIR spectra (Fig. 2) exhibit a qualitatively different and considerably more complex spectral signature than seen for 2DIR spectra of isolated vibrational resonances in condensed phases [24–27]. The sign change and spacing between the center of red and blue overlapping “X”s at the shorter T_w ’s identifies the red (positive) and blue (negative) 2DIR features resulting from GSB-SE and ESA contributions to the $\text{N}_2\text{O}/\text{SF}_6$ 2DIR spectra. The elongated spectral shape along the diagonal ($\omega_1 = \omega_3$) and the parallel component redshifted in the ω_3 direction by the $\nu_3 1 \rightarrow 2$ transition anharmonicity ($\sim 28 \text{ cm}^{-1}$) at $T_w = 0.2$ ps, are the well-known signatures of an inhomogeneously broadened vibrational band in

2DIR spectra. The corresponding antidiagonal features seen in these quasifree rotor spectra are unique relative to previous 2DIR results; however, they are reminiscent of the 2DIR spectrum predicted for two anticorrelated inhomogeneously broadened coupled oscillators [28,29]. The “X” pattern is evident in a prior 2D rovibronic, low density coherent 4-wave mixing spectroscopy that assists interpretation and simplification of gas phase spectra [30].

Dramatic changes are seen in these 2DIR spectra (Figs. 2, and S2 of Ref. [19]) as a function of T_w . All the initial ($T_w = 0.2$ ps) elongated features approach nearly symmetrical shapes at longer T_w ’s which is the well-known signature of transition frequency memory loss, characteristic of spectral diffusion processes in liquid phase environments. Furthermore, the eight spectral features in the 2DIR spectra (4 bleach and 4 absorption types) at the earliest T_w ’s evolve to 4 distinct features at $T_w \geq 30$ ps.

As shown previously, a change in the aspect ratio of the 2DIR spectral line shapes corresponding to the $a \rightarrow b$ transition as a function of T_w closely captures the decay of the FFCF [18]. Thus, the center line slope (CLS), also plotted in Fig. 2, experimentally determines FFCF for both the diagonal and antidiagonal GSB-SE components of the 2DIR spectra. The CLS decay has different signs for the diagonal and antidiagonal components, but both show the same dominant exponential decay constant within experimental error: 6.1 ± 0.3 ps (diagonal) and 5.8 ± 0.4 ps (antidiagonal). Similarly, the CLS decay times for the lower density ($\rho^* = 0.16$) sample (Fig. S3) are 9.4 ± 0.3 ps (diagonal) and 9.5 ± 0.6 ps (antidiagonal). However, best fits to all these experimental CLS decays also find a small ($\sim 5\%$ of total amplitude) positive constant component for the diagonal and anti-diagonal 2DIR GSB-SE features. This small residual offset or very slow

Ground State Bleach Pathways



Excited State Absorption Pathways

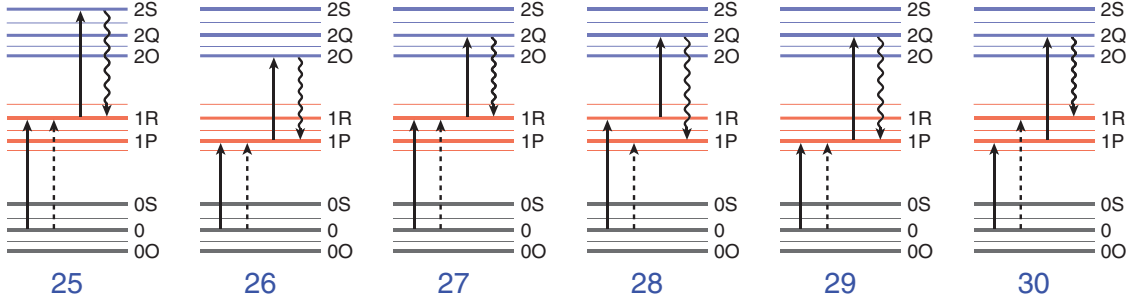


FIG. 3. Twelve (six GSB-SE and six ESA) of the thirty-six density matrix pathways contributing to the 2DIR signal originating in the $v = 0$, J rovibrational level are highlighted.

fluctuation component may be attributable to pure vibrational dephasing processes (here due to a static inhomogeneity on the experimental time scale), sample heating effects or consequences of the canceling effects of adjacent, oppositely signed 2DIR contributions.

In order to capture the essential features of the observed quasifree rotor 2DIR spectra, and provide a basis for interpreting the observed T_w dependence in terms of the underlying rotationally and vibrationally specific collision dynamics, a phenomenological model was developed. The 2DIR signal generated in the $k_s = k_{\text{probe}}$ direction for the pump-probe experimental configuration employed here is given by

$$S(k_s; \omega_3, T_w, \omega_1) \propto \text{Re} \left(\int_{-\infty}^{\infty} \int_{-\infty}^{\infty} R_{\text{Tot}}^{(3)}(\tau_3, T_w, \tau_1) e^{i\omega_1 \tau_1} e^{i\omega_3 \tau_3} d\tau_1 d\tau_3 \right), \quad (1)$$

where τ_1 , T_w , and τ_3 are the delays between the two pump pulses; the second pump and the probe pulses; and the $P^{(3)}$ signal detection time, respectively. Since the incident pulse durations (~ 85 fs) are much shorter than the dynamics observed here, only the intervals between pulse maxima are used for τ_1 , T_w , and τ_3 .

For a single vibrational resonance only a three level, optically coupled system, consisting of the ground ($v = 0$), and first and second ($v = 1, 2$) excited vibrational states, is needed to model the 2DIR signal. Consequently, six Liouville pathways, within the rotating wave approximation, due to spatially overlapped rephasing ($-k_{\text{pump}} + k_{\text{pump}} +$

k_{probe}) and nonrephasing ($+k_{\text{pump}} - k_{\text{pump}} + k_{\text{probe}}$) contributions result for well-separated pulses [31]. However, for an initial rotational level J in $v = 0$, i.e., $|0J\rangle$, an eight rovibrational level system, $|vJ\rangle$, is required to calculate the 2DIR spectrum of a quantum free rotor. A 2DIR signal pathway originating in $|0J\rangle$ ($\equiv 0$) has two accessible rovibrational levels in the $v = 1$ excited state ($|1J + 1\rangle \equiv 1R$ and $|1J - 1\rangle \equiv 1P$), three in the $v = 2$ second excited state ($|2J + 2\rangle \equiv 2S$, $|2J\rangle \equiv 2Q$, $|2J - 2\rangle \equiv 2O$) and three in the ground vibrational state ($|0J + 2\rangle \equiv 0S$, $|0J\rangle \equiv 0$, and $|0, J - 2\rangle \equiv 0O$) due to the $\Delta J = \pm 1$ selection rule for each $\Delta v = \pm 1$ dipole interaction in this third-order experiment. (See Fig. S4 of Ref. [19]). Consequently, there are six rovibrationally explicit Liouville pathways possible for each of the usually considered six types of Liouville pathways contributing to the 2DIR spectrum of an isolated vibrational oscillator [1,28]. Thus, the *total* third-order response function for the description of a 2DIR spectrum of a rovibrational resonance originating in a *single* rovibrational level for nonoverlapped pump and probe pulses is modeled as a sum of 36 rovibrationally explicit Liouville pathways:

$$R_{\text{Tot}}^{(3)}(\tau_3, T_w, \tau_1) = \sum_{n=1}^{36} R_n^{(3)}(\tau_3, T_w, \tau_1). \quad (2)$$

Twelve such representative pathways showing the temporal evolution from left to right of the density matrix elements contributing to the signal polarization [32–34] are shown in Fig. 3, and all 36 of these pathways are summarized in the Supplemental Material [19] (Fig. S6).

Expressions for the third-order responses contributing to vibrational 2DIR spectra have been described in detail previously [28], thus only those features most salient to their extension to this rovibrational system are summarized here. Each of the 36 contributing rovibrational response functions are a product of four path-specific transition moments, exponential oscillatory phase factors at the resonant transition frequencies during each of the interpulse evolution periods (τ_1, T_w, τ_3), and a path-specific nonlinear dephasing function [35,36]. The required dephasing functions can be written as products of exponentiated line shape functions, $g_{ab}(t)$, which are defined in terms of the $a \rightarrow b$ FFCF, $C_{a,b}(\tau_2 - \tau_1)$, within the second order cumulant expansion approximation [37]

$$g_{ab}(t) = \int_0^t d\tau_2 \int_0^{\tau_2} d\tau_1 C_{a,b}(\tau_2 - \tau_1). \quad (3)$$

The FFCF is determined by the underlying fluctuation dynamics of the system and is one of the key quantities determined by 2DIR spectral analysis [1,18]. The required rovibrationally explicit FFCFs are given by

$$C_{na,n'\beta}(t) = \langle \delta\omega_{n0}^\alpha(t) \delta\omega_{n'0}^\beta(0) \rangle = \zeta_{na,n'\beta} \Delta_{n0}^\alpha \Delta_{n'0}^\beta e^{-t/\tau_c}, \quad (4)$$

where n, n' refer to vibrational levels 0, 1, or 2, and α, β are the corresponding rotational branches. For $n, n' = 1$, $\alpha, \beta = P$, or R ($\Delta J = -1, +1$); for $n, n' = 0$ or 2, $\alpha, \beta = O, Q$, or S ($\Delta J = -2, 0$, or $+2$). In this stochastic Gaussian line broadening model [38], the time dependent fluctuations of the rovibrational transition frequencies, here due to gas collisions, $\delta\omega_{n0}^\alpha$, are defined relative to some corresponding ensemble averaged value ω_{n0}^α , i.e., $\omega_{n0}^\alpha(t) = \omega_{n0}^\alpha + \delta\omega_{n0}^\alpha(t)$. Δ_{n0}^α etc. [Eq. (4)], are the initial instantaneous widths of the corresponding $0 \rightarrow n$ rovibrational (α) branches, and τ_c is the transition energy fluctuation time scale. $\zeta_{na,n'\beta}$ is the correlation coefficient [28,39,40] describing the relative phasing of the fluctuations or distributions between $n\alpha, n'\beta$ rovibrational branches (see below). The total FFCF decay may result from multiple fluctuation mechanisms [Eq. (4)]. Although 14 rovibrationally explicit FFCFs, $C_{na,n'\beta}(t)$, are formally required to calculate the 2DIR spectrum of a free rotor, these may all be given in terms of three, unique $0 \rightarrow 1$ rovibrational FFCFs: $C_{1R,1R}(t), C_{1P,1P}(t)$, and $C_{1R,1P}(t)$, assuming negligible fluctuation in vibrational anharmonicity [28]; see Supplemental Material [19].

In order to capture the effects of spectral diffusion within the unresolved N_2O ν_3 rovibrational branches (Fig. 1) $\omega_{10}^{R^o}$ and $\omega_{10}^{P^o}$ are taken as the transition energy at each of the two ν_3 fundamental absorption branch maxima, and Δ_{10}^P and Δ_{10}^R are the corresponding inhomogeneous breadths of the P and R branches (Fig. 1). The branch maxima correspond to the $P(15)$ and $R(15)$ transition frequencies at 313 K and thus $J = 15$ is taken to be the initial rotational level in the

ground vibrational state in this 2DIR rovibrational analysis. This treatment is analogous to modeling the line broadening of a single vibrational oscillator due to solvent fluctuations of the vibrational energy gaps about an ensemble averaged vibrational transition frequency and the loss of frequency memory for a single vibrational oscillator (spectral diffusion). This rovibrational model, equivalently, allows for J memory loss or J spectral diffusion [37,38] due to bath interactions (collisions).

The ratio of $1 \rightarrow 2$ and $0 \rightarrow 1$ vibrational transition moments, given within the Condon approximation, used in this calculation is $\sqrt{1.6}$ as evident in the observed pump-probe responses and the rotational contribution to the rovibrational transition dipole is given by $\sqrt{\max(J, J')}$, where J and J' are the rotational quantum numbers of the rovibrational levels involved in the transition.

By definition, $\zeta_{na,n'\beta} = +1$ for autocorrelation functions ($\alpha = \beta$), $C_{1R,1R}(t)$ and $C_{1P,1P}(t)$. However, for the cross-correlation functions ($\alpha \neq \beta$), $\zeta_{1R,1P} = -1$ since for any J value, $\delta\omega_{10}^R(t)\delta\omega_{10}^P(0) < 0$ (see Eq. S9, Supplemental Material [19]) and, consequently, $C_{1R,1P}(t)$ is perfectly anticorrelated. Detailed expressions for each of the 36 response functions [$R_n^{(3)}(\tau_3, T_w, \tau_1)$] are given in the Supplemental Material [19].

Calculated 2DIR spectra for the ν_3 mode of N_2O in SF_6 ($\rho^* = 0.30$) resulting from the model outlined above are shown in Fig. 2 as a function of T_w and closely capture the structure of the experimental 2DIR spectra and their T_w dependence. The corresponding calculated linear absorption spectrum is shown in Fig. 1. Similar agreement between observed and calculated 2DIR results are found for the less dense $\rho^* = 0.16$ solution (Fig. S2). Parameters for these calculated 1D and 2D spectra are summarized in Table I and in the Supplemental Material [19]. The values of Δ_{10}^P and Δ_{10}^R were selected to capture the linear spectral shape in the central portion of the rovibrational absorption band (Figs. 1, and S1 of Ref. [19]). Given the Gaussian distribution of the instantaneous frequencies inherent to this line broadening model, poor fits in the wings of the experimental asymmetric rovibrational spectrum are expected. However, although not rigorously exact for capturing the shape of the instantaneous transition frequency distribution or any J -specific collision dynamics, the essential features of the observed linear and nonlinear

TABLE I. Summary of 2DIR experimental results and calculation parameters.

SF_6 Density	Δ_{10}^R (cm ⁻¹) ^a	Δ_{10}^P (cm ⁻¹) ^a	τ_c (ps) ^b	T_1 (ps) ^c	Z_{rot}
$\rho^* = 0.16$	17.7	21.4	9.5 ± 0.3	102	1.4
$\rho^* = 0.30$	19.3	22.4	6.0 ± 0.3	35	1.6

^aFWHM.

^bAverage of diagonal and antidiagonal CLS decay constant.

^cFastest component of biexponential lifetime decay.

spectra are well described by this analysis, and can be understood in terms of spectral diffusion and the rovibrationally specific 2DIR pathways (Fig. 3). In particular, the antidiagonal 2DIR spectral features evident for both the GSB-SE and ESA contributions at early times, and the observed J scrambling as a function of T_w are captured by this treatment. Subsequent more rigorous treatments of these 2DIR observations will have to take a full quantum level specific treatment of coherence loss and J -state changing dynamics into account.

The 36 rovibrational Liouville pathways give rise to twelve unique signal peaks in the 2DIR spectrum in this model. The twelve red (GSB-SE) and blue (ESA) labeled circles on the 2DIR spectral map in Fig. 4 indicate these signal locations and the number identifies a specific signal pathway from Fig. 3 contributing to the 2DIR spectrum at that (ω_1, ω_3) position. These signals are centered at the fundamental R (ω_{10}^R) and P (ω_{10}^P) branch transitions along the ω_1 axis and at 8 signal frequencies along the ω_3 detection axis (see Fig. 4). However, due to the small dependence of rotational constants on vibrational level ($B_0 \approx B_1 \approx B_2$) and lack of discrete rotational resolution at these densities, only 4 signal frequencies are distinguishable along ω_3 : $\omega_{10}^R \approx \omega_{10}^{R'}$, $\omega_{10}^P \approx \omega_{10}^{P'}$, $\omega_{21}^R \approx \omega_{21}^{R'}$, and $\omega_{21}^P \approx \omega_{21}^{P'}$ (See Supplemental Material [19], Fig. S7). Hence, in contrast to the 2DIR spectra of isolated vibrational resonances in condensed phase environments characterized by a single T_w dependent GSB-SE and ESA spectral component, the 2DIR spectrum of a free rotor exhibits at least 4 GSB-SE and 4 ESA features. The elongated shapes observed at shorter T_w 's for these 8 2DIR spectral regions are due to the initial predominant inhomogeneous character due to the ensemble of J -specific allowed rovibrational transitions.

Arguably, the most obvious signature in a 2DIR spectrum of free rotor character are the antidiagonally elongated

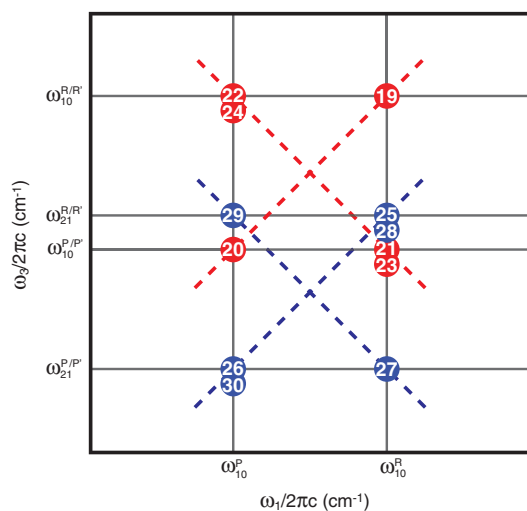


FIG. 4. 2DIR map that indicates where signal polarization is generated by the 12 density matrix pathways in Fig. 3 as a function of (ω_1, ω_3) .

spectral features, which result in X-like cross peaks at early times (Figs. 2 and 4). These features result from the inherent perfectly anticorrelated cross-correlation contributions, $\zeta_{1R,1P} = -1$, i.e., where $C_{1R,1P}(t) = \langle \delta\omega_{10}^R(t)\delta\omega_{10}^P(0) \rangle = -\Delta_{10}^R\Delta_{10}^P e^{-t/\tau_c}$. Such perfectly anticorrelated FFCFs are unique to this quantum rotor description. The diagonally and antidiagonally elongated line shapes at early T_w 's, symmetrize at longer times as observed both in the experiments and calculations. Only 4 spectral features are evident at longer T_w 's because the N_2O ν_3 vibrational anharmonicity (28 cm^{-1}) almost exactly matches the frequency difference between P and R branch maxima (25 cm^{-1}). Consequently, the symmetrized diagonal GSB-SE contribution of the P transition (pathway 20) almost exactly cancels the (P,R) ESA cross-peak (pathway 29), and the cross peak (R, P) GSB-SE signals (pathways 21, 23) effectively cancel the ESA of the R transitions (pathways 25 and 28). Such intensity cancellation from these same signal polarization pathways results in the two nodes at approximately $(\omega_{10}^P, \omega_{21}^R)$ and $(\omega_{10}^R, \omega_{21}^P)$ in the earliest time 2DIR spectra (Fig. 2).

Aside from capturing the 2DIR spectral line shapes for a free rotor, this analysis reveals that the loss of J memory or rotational spectral diffusion due to N_2O - SF_6 interactions is dominated by an exponential decay process with time constants of 9.4 and 6.0 ps at $\rho^* = 0.16$ and 0.30, respectively. Mean free times between N_2O and SF_6 collisions (τ_{coll}) based on hard sphere calculations are correspondingly 7.0 and 3.8 ps at the experimental state points (see Supplemental Material [19]) [41–43]. Thus, rotational equilibration ($Z_{\text{rot}} = \tau_c/\tau_{\text{coll}}$) occurs within 1 to 2 collisions in these moderately dense gas mixtures; $Z_{\text{rot}} = 1.4$ ($\rho^* = 0.16$) and 1.6 ($\rho^* = 0.30$) and is therefore a highly efficient process at near ambient temperatures. From low pressure emission, state resolved transient absorption or ultrasonic measurements, Z_{rot} has been previously typically found to be in the range of 1 or 2 for polar molecules, and 4–5 for nonpolar molecules (hydrides excepted) [44,45]. Thus, the results of this 2DIR analysis provides quantitative direct time measurements of rotational relaxation that are consistent with these prior low density results. However, the ultrafast nonlinear methodology provides such quantitative relaxation measurements for much higher pressure regimes. These high density 2DIR CLS decays and NMR based determinations of angular momentum correlation times should provide an interesting comparison of these direct and indirect measures of rotational relaxation [46,47]. This 2DIR methodology for quasifree rotors can be applied to studies of the effects of different types of solvent interactions on rotational relaxation rates, studies of the onset of liquid-like character and dynamics in near critical point regions, as well as reactivity and relaxation in high pressure and high temperature environments.

This material is based upon work supported by the National Science Foundation under CHE-1152797 and CHE-1609952.

*Corresponding author.

lziegler@bu.edu

†Present Address: Department of Chemistry, Northwestern University, Evanston IL 60208, USA.

- [1] P. Hamm and M. Zanni, *Concepts and Methods of 2D Infrared Spectroscopy* (Cambridge University Press, 2011).
- [2] M. Cho, *Chem. Rev.* **108**, 1331 (2008).
- [3] M. D. Fayer, D. E. Moilanen, D. Wong, D. E. Rosenfeld, E. E. Fenn, and S. Park, *Accounts Chem. Res.* **42**, 1210 (2009).
- [4] S. T. Roberts, K. Ramasesha, and A. Tokmakoff, *Accounts Chem. Res.* **42**, 1239 (2009).
- [5] K. Ramasesha, L. De Marco, A. Mandal, and A. Tokmakoff, *Nat. Chem.* **5**, 935 (2013).
- [6] A. Mandal, K. Ramasesha, L. De Marco, and A. Tokmakoff, *J. Chem. Phys.* **140**, 204508 (2014).
- [7] M. Thämer, L. De Marco, K. Ramasesha, A. Mandal, and A. Tokmakoff, *Science* **350**, 78 (2015).
- [8] A. Mandal and A. Tokmakoff, *J. Chem. Phys.* **143**, 194501 (2015).
- [9] T. Elsaesser, *Accounts Chem. Res.* **42**, 1220 (2009).
- [10] M. Fayer, *Annu. Rev. Phys. Chem.* **60**, 21 (2009).
- [11] C. R. Baiz, P. L. McRobbie, J. M. Anna, E. Geva, and K. J. Kubarych, *Accounts Chem. Res.* **42**, 1395 (2009).
- [12] M. T. Zanni and R. M. Hochstrasser, *Curr. Opin. Struct. Biol.* **11**, 516 (2001).
- [13] S. Woutersen and P. Hamm, *J. Phys. Condens. Matter* **14**, R1035 (2002).
- [14] Z. Ganim, H. S. Chung, A. W. Smith, L. P. DeFlores, K. C. Jones, and A. Tokmakoff, *Accounts Chem. Res.* **41**, 432 (2008).
- [15] C. S. Peng, K. C. Jones, and A. Tokmakoff, *J. Am. Chem. Soc.* **133**, 15650 (2011).
- [16] C. H. Giammanco, P. L. Kramer, S. A. Yamada, J. Nishida, A. Tamimi, and M. D. Fayer, *J. Chem. Phys.* **144**, 104506 (2016).
- [17] F. Perakis, S. Widmer, and P. Hamm, *J. Chem. Phys.* **134**, 204505 (2011).
- [18] K. Kwak, S. Park, I. J. Finkelstein, and M. D. Fayer, *J. Chem. Phys.* **127**, 124503 (2007).
- [19] See Supplemental Material at <http://link.aps.org/supplemental/10.1103/PhysRevLett.120.103401> for details of experimental and calculation methods, FTIR and 2DIR results for N₂O in SF₆ at lower density ($\rho^* = 0.16$) and calculation of collision frequencies.
- [20] G. Herzberg, *Infrared and Raman Spectroscopy of Polyatomic Molecules* (Van Nostrand, New York, 1954).
- [21] G. Herzberg and L. Herzberg, *J. Chem. Phys.* **18**, 1551 (1950).
- [22] J. T. Shattuck, J. R. Schneck, L. R. Chieffo, S. Erramilli, and L. D. Ziegler, *J. Phys. Chem. B* **117**, 15774 (2013).
- [23] J. Helbing and P. Hamm, *J. Opt. Soc. Am. B* **28**, 171 (2011).
- [24] J. J. Loparo, S. T. Roberts, and A. Tokmakoff, *J. Chem. Phys.* **125**, 194521 (2006).
- [25] T. Steinel, J. B. Asbury, S. A. Corcelli, C. P. Lawrence, J. L. Skinner, and M. D. Fayer, *Chem. Phys. Lett.* **386**, 295 (2004).
- [26] A. Ghosh, A. Remorino, M. J. Tucker, and R. M. Hochstrasser, *Chem. Phys. Lett.* **469**, 325 (2009).
- [27] M. W. Nydegger, S. Dutta, and C. M. Cheatum, *J. Chem. Phys.* **133**, 134506 (2010).
- [28] M. Khalil, N. Demirdöven, and A. Tokmakoff, *J. Phys. Chem. A* **107**, 5258 (2003).
- [29] N.-H. Ge, M. T. Zanni, and R. M. Hochstrasser, *J. Phys. Chem. A* **106**, 962 (2002).
- [30] P. C. Chen, *J. Phys. Chem. A* **114**, 11365 (2010).
- [31] K. Kwak, J. Zheng, H. Cang, and M. D. Fayer, *J. Phys. Chem. B* **110**, 19998 (2006).
- [32] D. Lee and A. C. Albrecht, in *Advances in infrared and Raman Spectroscopy*, edited by R. J. H. Clark and R. E. Hester, (John Wiley & Sons, New York, 1985), p. 179.
- [33] M. Khalil and A. Tokmakoff, *Chem. Phys.* **266**, 213 (2001).
- [34] Y. Kwon, C. Lee, and S. Park, *Chem. Phys.* **445**, 38 (2014).
- [35] K. Ramasesha, L. De Marco, A. D. Horning, A. Mandal, and A. Tokmakoff, *J. Chem. Phys.* **136**, 134507 (2012).
- [36] J. Sung and R. J. Silbey, *J. Chem. Phys.* **115**, 9266 (2001).
- [37] S. Mukamel, *Nonlinear Optical Spectroscopy* (Oxford University Press, Oxford, 1995).
- [38] R. Kubo, *Advances in Chemical Physics* (John Wiley & Sons, Inc., New York, 1969), p. 101.
- [39] N. Demirdöven, M. Khalil, and A. Tokmakoff, *Phys. Rev. Lett.* **89**, 237401 (2002).
- [40] N. Demirdöven, M. Khalil, O. Golonzka, and A. Tokmakoff, *J. Phys. Chem. A* **105**, 8025 (2001).
- [41] NIST Chemistry WebBook, Standard Reference Database Number 69, National Institute of Standards and Technology, Gaithersburg MD, <http://webbook.nist.gov/chemistry/>.
- [42] C. J. Jameson and A. K. Jameson, *J. Chem. Phys.* **88**, 7448 (1988).
- [43] J. Yardley, *Introduction to Molecular Energy Transfer* (Academic Press, New York, 1980).
- [44] R. G. Gordon, W. Klemperer, and J. I. Steinfeld, *Annu. Rev. Phys. Chem.* **19**, 215 (1968).
- [45] P. K. Cheo and R. L. Abrams, *Appl. Phys. Lett.* **14**, 47 (1969).
- [46] J. DeZwaan and J. Jonas, *J. Chem. Phys.* **63**, 4606 (1975).
- [47] T. Yamaguchi, N. Matubayasi, and M. Nakahara, *J. Phys. Chem. A* **108**, 1319 (2004).